



The structural, dielectric, and magnetic properties of GdMnO₃ multiferroic ceramics

Fengjiao Ye¹ · Haiyang Dai¹ · Manman Wang¹ · Jing Chen¹ · Tao Li¹ · Zhenping Chen¹

Received: 19 November 2019 / Accepted: 13 January 2020 / Published online: 20 January 2020
© Springer Science+Business Media, LLC, part of Springer Nature 2020

Abstract

GdMnO₃ (GMO) ceramics were prepared by solid-state reaction method, the structure, defects, dielectric, and magnetic properties of GMO ceramics sintered at different temperatures have been studied. Characterization by XRD indicates that impurity phase-free GMO can be synthesized at 1350 °C. SEM measurements show that the grain size of GMO increases and the microstructure becomes denser with increasing sintering temperature. Positron annihilation results reveal that the vacancies concentration decreases when sintering temperature increases from 1300 to 1350 °C, and then increases when sintering temperature increases from 1350 to 1400 °C. Dielectric measurements indicate that the GMO ceramic sintered at 1350 °C presents higher dielectric constant and smaller dielectric loss. Magnetic properties measurements show that the magnetic properties of GMO can be modulated by sintering temperature. The relation between structure and properties implies that the cation vacancy defect has remarkable effects on the dielectric and magnetic properties of GMO.

1 Introduction

Multiferroic materials with the simultaneous coexistence of ferromagnetic and ferroelectric in the same phase have attracted extensive attention in recent years because of their potential applications and rich physical properties [1–5]. As a typical rare earth manganites, GdMnO₃ (GMO) is an interesting material due to its complex low-temperature magnetic ordering, magnetic frustration-induced ferroelectricity, and big magnetoelectric coefficient [6–8]. GMO with orthorhombic distorted perovskite structure exhibits metamagnetic features with lowering of temperature; it transforms from a paramagnetic phase to an antiferromagnetic phase at approximately 45 K, and then from antiferromagnetic to weak ferromagnetism (canted antiferromagnetism) at approximately 25 K. After that, the long-range ordering of the Gd³⁺ moments is appeared at approximately 6 K [6–9]. Although GMO displays rich physical implications and broad application prospects, the ferroelectric origin, complex low-temperature magnetic orderings, and magnetoelectric coupling mechanism remain indistinct. Therefore,

considerable attempts had been made to explore the internal physical mechanism of GMO.

It is well known that the relationship between structure and properties is the core of materials science, and the properties of materials strongly depend on its microstructure. The microstructure of materials can be modified greatly by synthesis method, synthesis parameters, doping, magnetic field, external pressure, etc. Recently, many attempts have been taken to study the effects of structure on the physical properties of GMO system [10–13]. Nandy et al. [11] investigated the structure and the magnetic properties of GMO system by doping Na at Gd site, which indicates that the decrease of structural distortion causes the increase of magnetic transition temperature and ferromagnetic interaction. The influences of external pressure on the ferroelectricity of GMO studied by Noda show that external pressure weakens the ferroelectricity of GMO [12]. Moreira [13] et al. found that the increase of the MnO₆ tilt angle induced by applied magnetic field leads to a weakening of the ferromagnetic exchange interaction in GMO. The above results indicate that the physical properties of GMO have intimate relationship with the microstructure.

The synthesis parameter is the key factor which can influence greatly the microstructure and properties for ceramic materials. The ceramics synthesized under the same preparation technique but different synthesis parameters display different structures and physical properties. Therefore, careful

✉ Haiyang Dai
dhyzhengzhou@163.com

¹ School of Physics and Electronic Engineering, Zhengzhou University of Light Industry, Zhengzhou 450002, China

study and optimization of synthesis parameters are required to obtain high-performance materials and reveal the inherent physical mechanism. In fact, the defects, especially of the vacancy-type, are inevitable to exist in ceramic materials, and they have intimate relationships with some properties of ceramic materials [14]. So, the impact of vacancy defects on the physical properties should not be neglected. GMO is a strongly correlated electron system, and the electric and magnetic properties of GMO are closely related to the electron structure and vacancy defects features. Furthermore, no systematic research upon the vacancy defect features of GMO system has been reported. In the present paper, the polycrystalline bulk materials of GMO were prepared by the solid-state reaction method, and positron annihilation technology was introduced to investigate the vacancy defects features in the synthesized ceramics. The influences of sintering temperature on the structure, microtopography, defects, electric, and magnetic performances of GMO system were systematically studied.

2 Experimental details

Polycrystalline GdMnO_3 (GMO) compounds were synthesized using solid-state reaction method. High-purity starting powders of Gd_2O_3 (Aladdin; purity, 99.99%; particle size, < 100 nm; density, 7.4 g/cm^3 ; quantity, 100 g per bottle) and Mn_2O_3 (Xiya Reagent; purity, 99.99%; particle size, $1.5 \mu\text{m}$; density, 4.8 g/cm^3 ; quantity, 25 g per bottle) with stoichiometric amounts were adequately ground for 6 h using ethanol as a medium and thoroughly mixed. The obtained powders were calcined at 1000 and 1250 °C for 24 h, respectively. After that, the calcined mixtures were finely ground for 2 h and pressed into small discs under a pressure of 9 MPa. Finally, these discs with 11 mm in diameter and 1.5–1.7 mm in thickness were sintered at 1300 °C, 1350 °C, and 1400 °C for 24 h, respectively.

The crystal structure information of the GMO ceramics synthesized at different temperatures were collected using XRD (Bruker D8) within a range of 20° to 70° with a 2θ step of 0.02° at room temperature. The microstructural characterization of the samples was studied by a scanning electron microscopy (SEM, JSM-6490LV). The positron annihilation spectroscopy (PAS) was carried out by a fast-fast coincidence lifetime spectrometer at room temperature ($20 \pm 0.5^\circ \text{C}$) with a $13 \mu\text{Ci } ^{22}\text{Na}$ as positron source. The obtained spectra with 10^6 counts were evaluated by using PATFIT program. The dielectric measurements were carried out using an impedance analyzer (Agilent HP 4194 A) at room temperature in the frequency range of 100 Hz–1 MHz. The magnetic measurements were performed by a superconducting quantum interference device magnetometer within

the temperature of 5–300 K under -5 kOe to 5 kOe external magnetic field.

3 Results and discussion

The X-ray power diffraction patterns of GMO multiferroic ceramics synthesized at different temperatures are depicted in Fig. 1. The sharp and distinct peaks indicate that the crystallinity of all GMO samples is good, and the peaks of all ceramics can be indexed as the orthorhombic structure with the Pnma space group. The figure also shows that the sample sintered at 1300 °C showed some weaker impurity phases of Gd_2O_3 and Mn_2O_3 ; this represents that Gd and Mn oxides did not completely transform to take part in the formation of the single-phase GMO compound [15]. The appearance of Gd_2O_3 and Mn_2O_3 illustrates that 1300 °C is not the optimum sintering temperature to synthesize the single-phase GMO. As the sintering temperature increases to 1350 °C, the impurity phases of Gd_2O_3 and Mn_2O_3 peaks have disappeared and GMO polycrystalline compounds with single phase are formed. The full width at half maximum (FWHM) of (112) peak for the samples sintered at 1300, 1350, and 1400 °C is 0.1556, 0.1353, and 0.1315°, respectively. It can be found that compared with the GMO ceramics synthesized at 1300 °C, the FWHM of the characteristic peaks for the samples synthesized at 1350 °C becomes sharper and the intensity of the characteristic peaks becomes stronger, indicating that GMO ceramics synthesized at 1350 °C have better crystallization and bigger grain size. The crystallite sizes of all the samples are obtained by considering the most intense diffraction peak in the pattern using Scherrer formula:

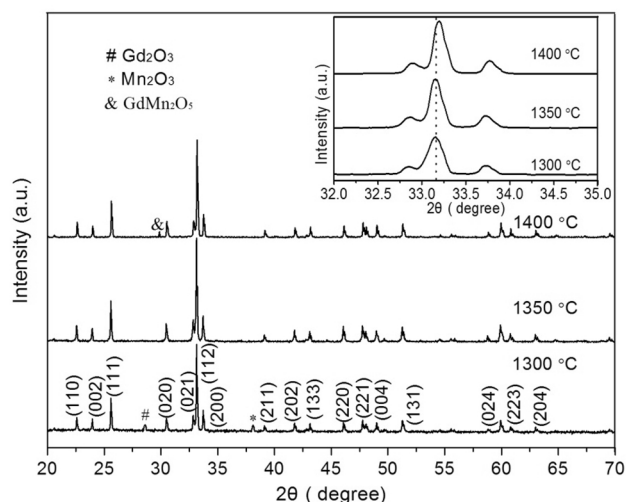


Fig. 1 XRD patterns of GdMnO_3 samples synthesized at different temperatures

$$D = \frac{K\lambda}{\beta \cos \theta} \quad (1)$$

where D is crystallite size, K (constant)=0.89, λ is the wave length of the incident radiation, β is the full width at half maximum in radians, and θ is the diffraction angle. Effects of strain, instruments, and other defects are ignored in the calculations. The crystallite sizes calculated by using Scherrer formula are 52, 60, 62 nm, respectively. It means that increasing the sintering temperature increases the crystallite size of the GMO samples. As the sintering temperature increases up to 1400 °C, a small amount of impurity phase of GdMn_2O_5 is observed along with gadolinium manganite [16], which may result from the decomposition of GMO at high-sintering temperature. The inset of Fig. 1 shows the peak in the range of 32.0–35.0°. It can be seen that the (112) peak position has no clear shift with the sintering temperature within the range of 1300–1350 °C, while the peak is shifted to higher 2θ angle as the sintering temperature increases from 1350 to 1400 °C, indicating a lattice contraction. It is well known that the polycrystalline samples have higher density of such disorder and defects, and the Mn ion in GMO ceramics usually has a mixed valence state ($\text{Mn}^{3+}/\text{Mn}^{4+}$) [17]. The lattice contraction may arise from the mixed valence state in the Mn-site.

The SEM images of GMO ceramics prepared at 1300, 1350, and 1400 °C are described in Fig. 2. The grain size, shape, and porosity of all GMO ceramics are significantly affected by sintering temperature. The SEM image of GMO samples synthesized at 1300 °C (as exhibited in Fig. 2a) is composed of a large amount of microscopic pores and grains with non-uniformly distributed size and irregular shapes. For the sample synthesized at 1350 °C (as exhibited in Fig. 2b),

the average grain size (2.41 μm) is much larger than that of the GMO ceramics synthesized at 1300 °C (0.98 μm), and the relatively uniformly distributed grains are separated by clear grain boundaries. A small amount of porosity can also be observed, but the size and amount are decreased as comparing with the GMO ceramics synthesized at 1300 °C. For the sample synthesized at 1400 °C (as exhibited in Fig. 2c), a compact microstructure with larger average grain size (3.65 μm) and no obvious pores can be observed. The grains of this sample are well linked by the well-defined grain boundaries. The average grain for all samples is larger than the crystallite size calculated from XRD analysis. This is due to the fact that the grains are constructed with several crystallites. The above results suggest that sintering temperature has important influences on the grain size, shape, and density of GMO multiferroic ceramics and an appropriate synthesizing temperature is conducive to enhance the microstructure of GMO-based ceramics.

Positron annihilation technique is a useful method to investigate the vacancy defects evolution in solid materials [18, 19]. The annihilation characteristic parameters of positrons can provide the vacancy defect information in the solids [18, 19]. The positron annihilation spectroscopy experiments were carried out at room temperature to study the defect characteristics in GMO ceramics. Due to the positron diffusion length in solids (about 100 nm) is much smaller than the grain size of the GMO ceramics, the positrons are mainly annihilated in the grains [20]. All of the spectra can be evaluated into two components with τ_1 , τ_2 lifetimes together with I_1 , I_2 ($I_1 + I_2 = 1$) relative intensities after subtracting source composition, as shown in Fig. 3. Based on the two-state trapping model, the shorter lifetime τ_1 is the reduced bulk positron lifetime, and the longer lifetime τ_2 is related to the annihilation of positron in defect

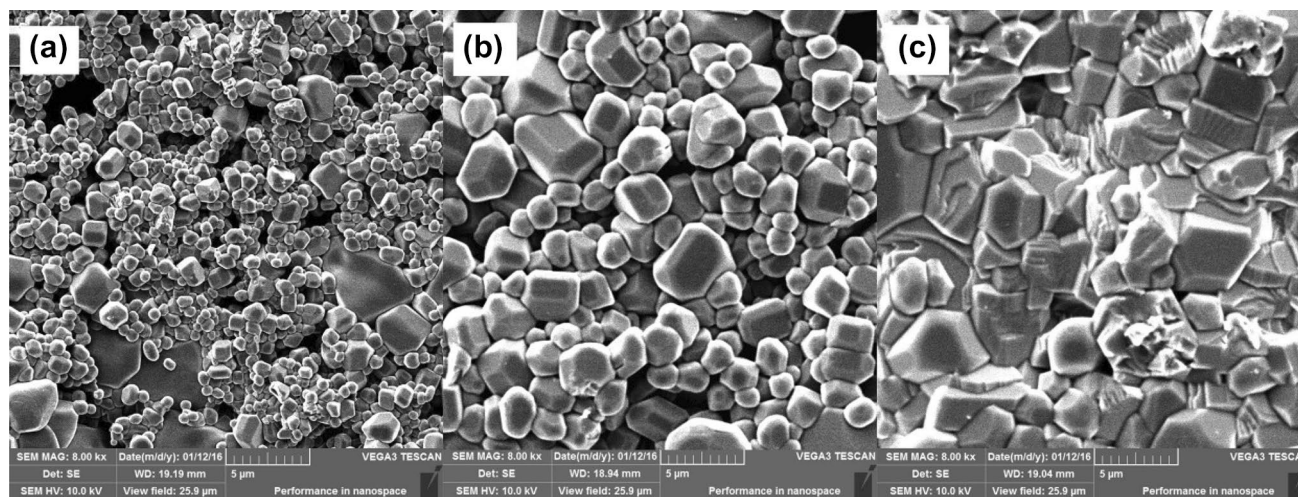


Fig. 2 SEM images of GdMnO_3 ceramics synthesized at different temperatures **a** 1300 °C **b** 1350 °C **c** 1400 °C

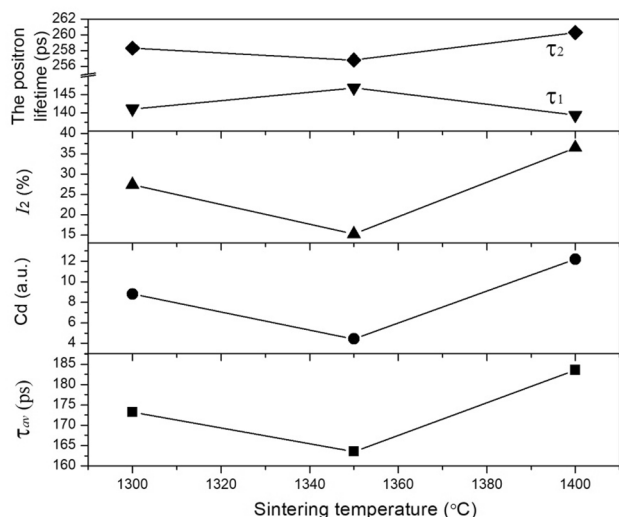


Fig. 3 Variation of positron lifetimes τ_1 , τ_2 , τ_{av} and intensity I_2 with sintering temperature for GdMnO₃ ceramics

states such as vacancies and vacancy clusters and represents the vacancy defect size [21, 22]. The relative intensity I_2 reflects the defect concentration in the samples.

Figure 3 shows the positron lifetimes τ_1 , τ_2 , τ_{av} and intensity I_2 in GMO ceramics synthesized at different temperatures. The values of τ_1 and τ_2 are in the range of 139–147 ps and 256–261 ps, respectively. The values of τ_1 and τ_2 are similar to the reported values of perovskite-type ceramic materials [14, 21, 22]. As shown in Fig. 3, it can be found that the value of τ_2 has a weak change with increasing sintering temperature, which means that the vacancy-type defect size in GMO ceramics is almost unaffected by sintering temperature. The reported positron lifetime in perfect TbMnO₃ lattice (bulk lifetime τ_b) is about 152 ps [23]. Gd and Tb ions are adjoining members of the lanthanum series. Therefore, the τ_b for perfect lattice of GdMnO₃ should be close to 152 ps. The ratio of defect lifetime to the bulk lifetime (τ_2/τ_b) can be used to evaluate the type of vacancy defects in semiconductors. It is assumed that the τ_2/τ_b values in the range of 1.1–1.3, 1.3–1.4, and > 1.5 are corresponding to positron annihilated in single vacancies, divacancies, and vacancy clusters, respectively. The calculated τ_2/τ_b value is 1.69, 1.68, and 1.71 for the samples synthesized at 1300, 1350, and 1400 °C, respectively, which mainly corresponds to vacancy clusters. The defect concentration C_d can be calculated using the following formula [24]:

$$C_d = \frac{I_2}{\mu} \left(\frac{1}{\tau_1} - \frac{1}{\tau_2} \right) \tag{2}$$

where μ is positron trapping coefficient. As shown in Fig. 3, the defect concentration C_d decreases with the increase in sintering temperature within the range of

1300–1350 °C, and then increases with the increase in sintering temperature within the range of 1350–1400 °C. The average lifetime (τ_{av}) presented in Fig. 3 is calculated as follows [25]:

$$\tau_{av} = \tau_1 I_1 + \tau_2 I_2 \tag{3}$$

τ_{av} is a universal stable and more reliable parameter, which can also reflect the evolution of the defect characters [25]. The variation of τ_{av} with sintering temperature is similar to that of C_d with sintering temperature. Therefore, the change of τ_{av} further confirms that the variation of vacancies concentration in GMO with sintering temperature.

To explore the dielectric behaviors of GMO ceramics, the variation of the dielectric constant (ϵ_r) and dielectric loss ($\tan\delta$) with frequency are collected at room temperature. Figure 4a exhibits the frequency-dependent dielectric constant for GMO ceramics synthesized at different temperatures. The ϵ_r for all of the samples decreases with increasing frequency in the low frequencies range, and it is almost constant in high frequencies range. The high dielectric constant in lower frequencies range might be related to the presence of all types of polarization (such as space charge polarization, ionic and electronic displacement polarization, and dipolar polarization) in GMO material. At higher frequencies, some of the polarizations cannot follow the applied electric field, so relaxation process is observed. Furthermore, the frequency stability of dielectric constant of the GMO ceramic synthesized at 1350 °C is better than the other samples. As shown in Fig. 4a, the dielectric constant at high frequencies of the GMO ceramic synthesized at 1350 °C is higher than that of the samples synthesized at 1300 and 1400 °C. Figure 4b exhibits the variation of $\tan\delta$ with frequency for GMO ceramics synthesized at different temperature. The frequency dependence of $\tan\delta$ for all GMO samples exhibits similar trend as that of ϵ_r . The $\tan\delta$ of the GMO ceramic synthesized at 1350 °C is smaller than that of the samples synthesized at 1300 and 1400 °C. Combined with the XRD, SEM, and positron annihilation results, it can be found that the sample synthesized at 1350 °C with good dielectric properties exhibits the single-phase structure, good crystallinity, better microstructure, and lower defects concentration. Therefore, it may be deduced that the dielectric properties of GMO system may be related to the phase structure, crystallinity, microstructure, and defects concentration.

The temperature-dependent magnetization ($M-T$) curves of the GMO samples synthesized at different temperatures under zero field cooled (ZFC) and field cooled (FC) modes measured with the external applied magnetic fields under 1 kOe are shown in Fig. 5. The magnetization of the samples synthesized at different temperatures measured under ZFC and FC modes are similar to each other. Literatures indicated

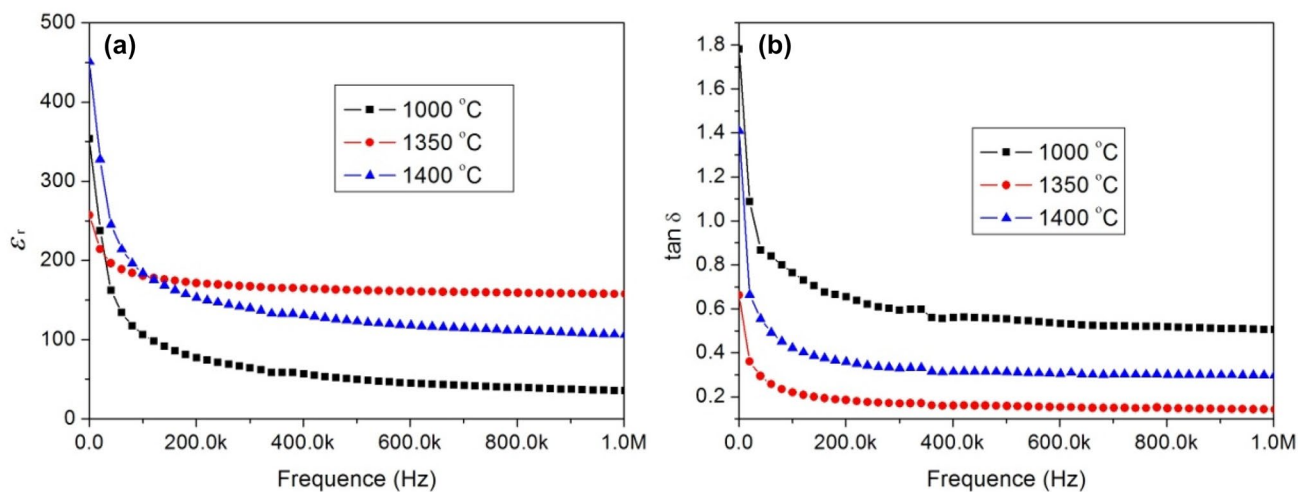


Fig. 4 Frequency-dependent dielectric constant (a) and dielectric loss (b) of GdMnO_3 ceramics synthesized at different temperatures

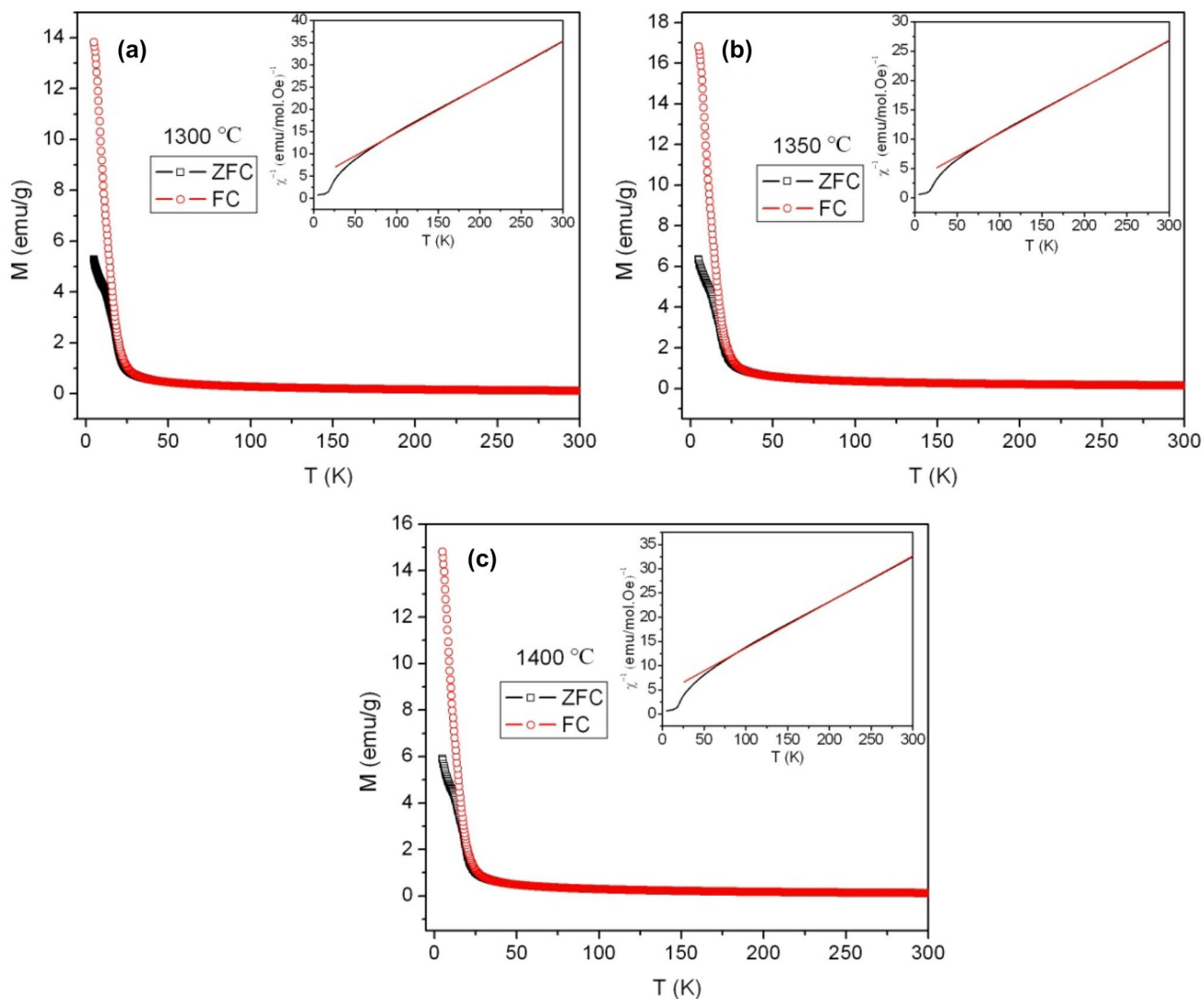


Fig. 5 M - T curves under ZFC and FC modes for the GdMnO_3 ceramics synthesized at different temperatures

that GMO showed a magnetic transition from paramagnetic (PM) to antiferromagnetic (AFM) at around 44 K due to the onset of antiferromagnetic ordering of Mn^{3+} spin ordering in GMO. However, the ZFC curves in our experiment do not display this magnetic transition due to the strongly paramagnetic moment of Gd^{3+} [17]. With decreasing the temperature, a rapid increase of magnetization in ZFC curves at approximately 24 K is corresponding to the transition from AFM to a weak ferromagnetism (canted AFM), which could result from the canted Mn^{3+} spin ordering and Gd 4f spin polarization [11, 17]. In addition, an anomaly is observed at approximately 8 K, which arises from the onset of an antiferromagnetic ordering of the gadolinium moments. It is believed that the magnetic structure at approximately 8 K is that the canted Gd^{3+} spins are antiparallel to the canted Mn^{3+} spins [11]. These results are consistent with previous reports [11]. However, in the FC curves, the magnetization for all samples increases suddenly at approximately 24 K, while the anomalies in the ZFC curves below 24 K are disappeared due to the enhancement of local field at gadolinium positions arising from ferromagnetic ordering of manganese moments [11, 26]. From the M – T curves, it can also be observed that the splitting between ZFC and FC curves below approximately 24 K which corresponds to the onset of weak ferromagnetism (canted AFM) and results from the competing between weak ferromagnetic and AFM behaviors in all samples [17]. The temperature of the splitting between ZFC and FC curves for GMO ceramics synthesized at 1300, 1350, and 1400 °C is about 23.5, 22.8, and 23.3 K, respectively. It can be found that sintering temperature has less influence on the weak ferromagnetism transition temperature. To study the magnetic interaction of GMO ceramics, the reciprocal of magnetic susceptibility ($1/\chi$) under ZFC mode is fitted by Curie–Weiss law. The variation of $1/\chi$ with temperature for all of the samples is shown in the inset of Fig. 5. The deviation between experimental data and theoretical fit is corresponding to the transition from paramagnetic to AFM [11]. The transition temperatures for the GMO ceramics synthesized at 1300, 1350, and 1400 °C are about 63.2, 61.2, and 68.0 K, respectively. The Curie–Weiss temperature (θ_{CW}) values evaluated from the $1/\chi$ – T curves at high temperature for the samples synthesized at 1300, 1350, and 1400 °C are negative suggesting that antiferromagnetic interactions display predominant in these samples [11, 17]. The above results are related with the Mn^{3+} – Mn^{3+} and Mn^{3+} – Mn^{4+} interactions, and the Jahn–Teller effect [11, 17].

To further explore the magnetic properties of the prepared GMO ceramics at low temperatures, the field dependence of magnetization (M – H) measurements were performed. The M – H curves for the GMO ceramics measured at 5 and 30 K are depicted in Fig. 6. The M – H curves at 30 K for all GMO ceramics show the linear field-dependent magnetization suggesting the antiferromagnetic behaviors of these samples. As

the measured temperature decreases to 5 K, the M – H curves of all GMO ceramics present a non-linear magnetic field-dependent magnetization with hysteresis, but they display unsaturation characteristic, which demonstrates that weak ferromagnetic and antiferromagnetic state coexist in all of the samples at 5 K. The magnetic structure at 5 K might be that the gadolinium moments are antiparallel to the canted manganese moments, and the canted Gd moment is higher than the canted Mn moment [11]. The M – H results are consistent with the M – T results. The shapes of the M – H curves at 5 K for the samples synthesized at different temperatures are similar with each other, but the maximum and remnant magnetization are different. The values of maximum magnetization are approximately 26.3, 33.4, and 28.9 emu/g for the GMO ceramics synthesized at 1300, 1350, and 1400 °C, respectively. The values of remnant magnetization are approximately 7.6, 9.4, and 8.3 emu/g for the GMO ceramics synthesized at 1300, 1350, and 1400 °C, respectively. It means that the GMO ceramic synthesized at 1350 °C has the biggest magnetization. A notable characteristic found by comparing Fig. 6 with Fig. 3 is that the magnetization GMO ceramics with the sintering temperature shows a similar change tendency as the vacancy defect concentration I_2 with the sintering temperature. It may be concluded that the magnetization for GMO system at 5 K has close relation with the cation vacancy defect concentration, and the cation vacancies concentration is a significant parameter which can influence dramatically the magnetization of GMO. As shown in Fig. 6, the samples synthesized at different temperatures represent ferromagnetic behavior at 5 K. The existence of cation vacancy in the ferromagnetic orders results in the decrease of magnetization. The GMO ceramic synthesized at 1350 °C has a lower vacancy defect concentration as compared to the GMO ceramics synthesized at 1300 and 1400 °C, hence it presents a higher magnetization. Besides the factors of defects, impurity phases and lattice distortion are also influence the magnetic behaviors of GMO. According to the XRD analysis, the GMO ceramic synthesized at 1350 °C form a single-phase structure which may also be benefit to improve the magnetic properties. At low temperature, GMO shows the spin frustration configuration, the degree of frustration can tune the magnetic behaviors of GMO [11]. From the XRD results, it could be found that the GMO ceramic sintered at 1400 °C shows lattice contraction as compared with the GMO ceramic sintered at 1350 °C. Therefore, the partial release of the spin frustration of GMO ceramic sintered at 1400 °C can also lead to a decrease in magnetization.

4 Conclusion

Polycrystalline GdMnO_3 samples are synthesized by the solid-state reaction at different sintering temperatures and characterized by XRD, SEM, positron annihilation

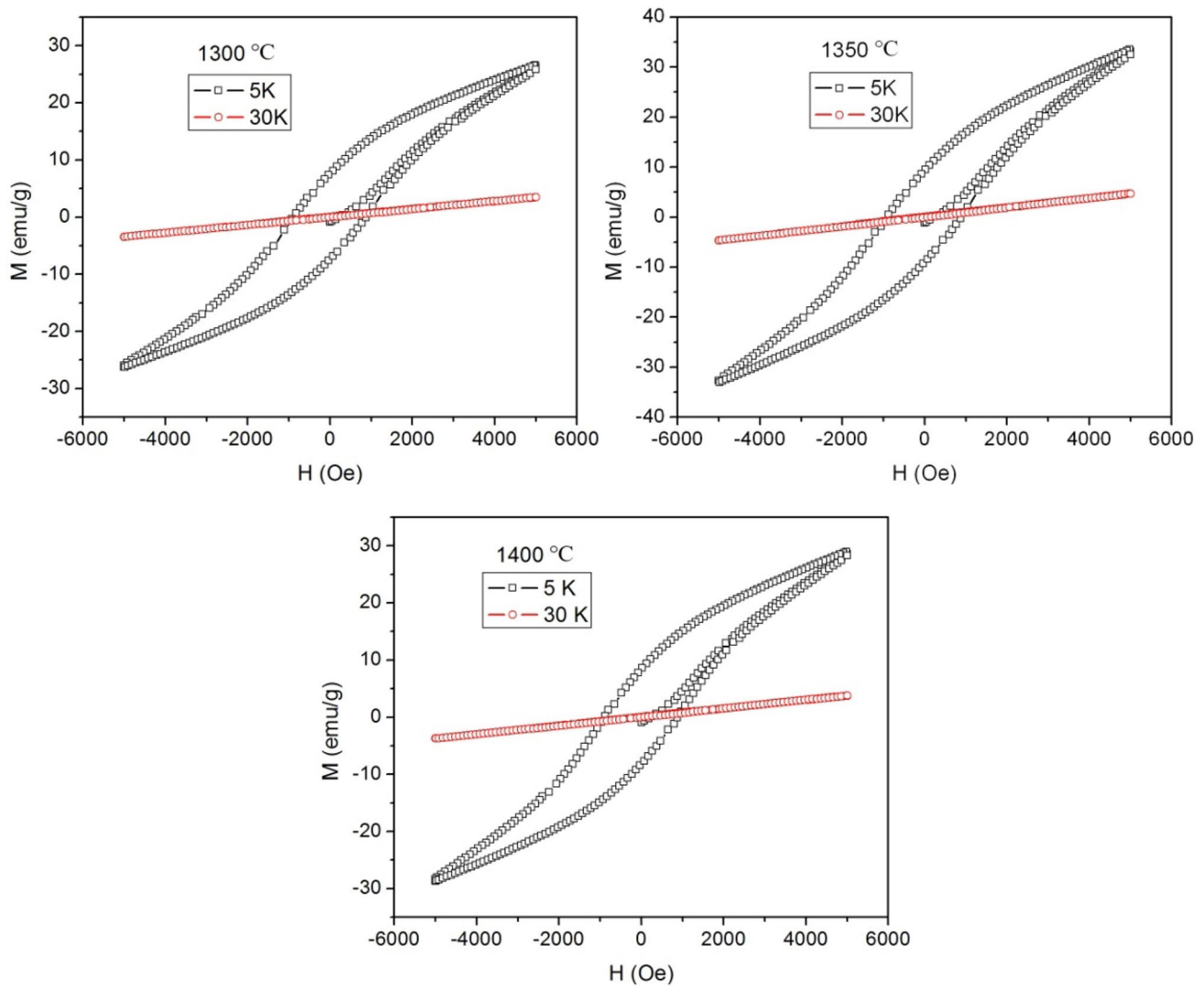


Fig. 6 M – H curves for the GdMnO_3 ceramics synthesized at different temperatures taken at 5 K and 30 K

spectroscopy technique, and superconducting quantum interference device magnetometer. XRD measurements show that the GdMnO_3 ceramic synthesized at 1350 °C has single-phase structure. SEM investigations indicate that a higher sintering temperature is favorable to prompt grain growth and improve the density of GdMnO_3 system. Positron annihilation spectroscopy analysis manifests that cation vacancy defects are existed in GdMnO_3 ceramics synthesized at different sintering temperatures; the vacancies defects size in GMO ceramics is almost unaffected by sintering temperature, while vacancies defects concentration has close relation with the sintering temperature. The studies of electric and magnetic properties indicate that sintering temperature obviously influence the dielectric constant, dielectric loss, magnetic transition temperature, and magnetization of GdMnO_3 , and appropriate sintering temperature is conducive to enhance the dielectric and magnetic behaviors of

GdMnO_3 system. The results above indicate that the cation vacancy defect has remarkable effects on the dielectric and magnetic behaviors of GdMnO_3 -based ceramics.

Acknowledgements This work is supported by the National Natural Science Foundation of China (Nos. 11775192, 11675149), and Key Scientific Research Project of Colleges and Universities in Henan Province (No. 18A140035).

References

1. S. Dong, J.M. Liu, S.W. Cheong, Z.F. Ren, Multiferroic materials and magnetoelectric physics: symmetry, entanglement, excitation, and topology. *Adv. Phys.* **64**, 519–626 (2015)
2. M.S. Alam, R. Hossain, M.A. Basith, Enhanced multiferroism in Gd-doped BiMn_2O_5 ceramics. *Ceram. Int.* **44**, 594–1602 (2018)

3. A.K. Kundu, M. MotinSeikh, P. Nautiyal, Bismuth centred magnetic perovskite: a projected multiferroic. *J. Magn. Magn. Mater.* **378**, 506–528 (2015)
4. S. Liu, S.Q. Yan, H. Luo, L.L. Yao, Z.W. Hu, S.X. Huang, L.W. Deng, *J. Mater. Sci.* **53**, 1014–1023 (2018)
5. R. Choithrani, M.N. Rao, S.L. Chaplot, N.K. Gaur, R.K. Singh, Lattice dynamics of manganites RMnO_3 (R=Sm, Eu or Gd): instabilities and coexistence of orthorhombic and hexagonal phases. *New J. Phys.* **11**, 073041-1–073041-14 (2009)
6. A.M. Kadomtseva, Y.F. Popov, G.P. Vorobev, K.I. Kamilov, A.P. Pyatakov, V.Y. Ivanov, A.A. Mukhin, A.M. Balbashov, Specificity of magnetoelectric effects in a new GdMnO_3 magnetic ferroelectric. *JETP Lett.* **81**, 19–23 (2005)
7. L. Lin, L. Li, Z.B. Yan, Y.M. Tao, S. Dong, J.M. Liu, Ferroelectricity of polycrystalline GdMnO_3 and multifold magnetoelectric responses. *Appl. Phys. A* **112**, 947–954 (2013)
8. T. Kimura, G. Lawes, T. Goto, Y. Tokura, A.P. Ramirez, Magnetoelectric phase diagrams of orthorhombic RMnO_3 (R=Gd, Tb, and Dy). *Phys. Rev. B* **71**, 224425-1–224425-13 (2005)
9. K. Noda, S. Nakamura, J. Nagayama, H. Kuwahara, Magnetic field and external-pressure effect on ferroelectricity in manganites: comparison between GdMnO_3 and TbMnO_3 . *J. Appl. Phys.* **97**, 10C103-1–10C103-3 (2005)
10. N.R. Qu, Z.P. Li, A novel wet-chemical route for synthesis of multiferroic AMnO_3 (A= Gd, Tb, Dy) particles and its structural, optical and magnetic properties. *J. Supercond. Nov. Magn.* **31**, 2869–2877 (2018)
11. A. Nandy, A. Roychowdhury, T. Kar, D. Das, S.K. Pradhan, Effect of sodium doping on the microstructure, lattice distortion and magnetic properties of GdMnO_3 tiny single crystals. *RSC Adv.* **6**, 20609–20620 (2016)
12. A. Pal, P. Murugavel, Impact of cationic vacancies on the physical characteristics of multiferroic GdMnO_3 . *J. Appl. Phys.* **123**, 234102-1–234102-9 (2018)
13. J.A. Moreira, A. Almeida, M.R. Chaves, J. Kreisel, J. Oliveira, F. Carpinteiro, P.B. Tavares, Magnetically-induced lattice distortions and ferroelectricity in magnetoelectric GdMnO_3 . *J. Phys.* **24**, 436002-1–436002-6 (2012)
14. D.J. Keeble, S. Singh, R.A. Mackie, M. Morozov, S. McGuire, D. Damjanovic, Cation vacancies in ferroelectric PbTiO_3 and $\text{Pb}(\text{Zr}, \text{Ti})\text{O}_3$: a positron annihilation lifetime spectroscopy study. *Phys. Rev. B* **76**, 144109-1–144109-5 (2007)
15. S. Samantaray, D.K. Mishra, S.K. Pradhan, P. Mishra, B.R. Sekhar, D. Behera, P.P. Rout, S.K. Das, D.R. Sahu, B.K. Roul, Correlation between structural, electrical and magnetic properties of GdMnO_3 bulk ceramics. *J. Magn. Magn. Mater.* **339**, 168–174 (2013)
16. D. Singh, R. Gupta, K.K. Bamzai, Electrical and magnetic properties of $\text{GdCr}_x\text{Mn}_{1-x}\text{O}_3$ ($x=0.0, 0.1$) multiferroic nanoparticles. *J. Mater. Sci.* **28**, 5295–5307 (2017)
17. D.J. Keeble, S. Wicklein, R. Dittmann, L. Ravelli, R.A. Mackie, W. Egger, Identification of A- and B-site cation vacancy defects in perovskite oxide thin films. *Phys. Rev. Lett.* **1105**, 226102-1–226102-4 (2010)
18. P.Y. Raval, P.R. Pansara, N.H. Vasoya, K.B. Modi, P.M.G. Nambissan, Positron annihilation spectroscopic investigation of high energy ball-milling engendered defects in $\text{CaCu}_3\text{Ti}_4\text{O}_{12}$. *Ceram. Int.* **44**, 15887–15895 (2018)
19. G.L. Yuan, C. Li, J. Yin, Z.G. Liu, D. Wu, A. Uedono, Positron annihilation studies on the behaviour of vacancies in $\text{LaAlO}_3/\text{SrTiO}_3$ heterostructures. *J. Phys. D* **45**, 445305-1–445305-5 (2012)
20. T. Li, H.F. He, T. Zhang, B. Zhao, Z.Q. Chen, H.Y. Dai, R.Z. Xue, Z.P. Chen, Effect of synthesizing temperatures on the microstructure and electrical property of $\text{CaCu}_3\text{Ti}_4\text{O}_{12}$ ceramics prepared by sol-gel process. *J. Alloys Compd.* **684**, 315–321 (2016)
21. H.Y. Dai, T. Li, Z.P. Chen, D.W. Liu, R.Z. Xue, C.Z. Zhao, H.Z. Liu, N.K. Huang, Studies on the structural, electrical and magnetic properties of Ce-doped BiFeO_3 ceramics. *J. Alloys Compd.* **672**, 182–189 (2016)
22. R.A. Mackie, A. Pelaiz-Barranco, D.J. Keeble, Vacancy defects in PbTiO_3 and lanthanide-ion-doped PbTiO_3 : A study of positron lifetimes. *Phys. Rev. B* **82**, 024113-1–024113-7 (2010)
23. D.J. Keeble, S. Wicklein, R. Dittmann, L. Ravelli, R.A. Mackie, W. Egger, Identification of A- and B-site cation vacancy defects in perovskite oxide thin films. *Phys. Rev. Lett.* **105**, 226102-1–226102-4 (2010)
24. T. Li, D.W. Liu, H.Y. Dai, H.W. Xiang, Z.P. Chen, H.F. He, Z.Q. Chen, Effect of defect on the nonlinear and dielectric property of $\text{Ca}_{(1-x)}\text{Sr}_x\text{Cu}_3\text{Ti}_4\text{O}_{12}$ ceramics synthesized by sol-gel process. *J. Alloys Compd.* **599**, 145–149 (2014)
25. H.F. He, B. Zhao, N. Qi, B. Wang, Z.Q. Chen, X.L. Su, X.F. Tang, Role of vacancy defects on the lattice thermal conductivity in In_2O_3 thermoelectric nanocrystals: a positron annihilation study. *J. Mater. Sci.* **53**, 12961–12973 (2018)
26. W.S. Ferreira, J.A. Moreira, A. Almeida, M.R. Chaves, J.P. Araujo, J.B. Oliveira, J.M.M.D. Silva, M.A. Sa, T.M. Mendonca, P.S. Carvalho, Spin-phonon coupling and magnetoelectric properties: EuMnO_3 versus GdMnO_3 . *Phys. Rev. B* **79**, 054303-1–054303-10 (2009)

Publisher's Note Springer Nature remains neutral with regard to jurisdictional claims in published maps and institutional affiliations.